Imperfections in amorphous chalcogenides. IV. A model of electrical conduction processes in amorphous and crystalline In_2Se_3

Yuichi Watanabe, Shuichi Kaneko, Hiroshi Kawazoe, and Masayuki Yamane
Department of Inorganic Materials, Tokyo Institute of Technology, Ohokayama, Meguro-ku, Tokyo 152, Japan
(Received 12 December 1988; revised manuscript received 3 April 1989)

Electrical conduction in amorphous In_xSe_{100-x} (a-In_xSe_{100-x}) thin films is examined, where x ranges from 35 to 44. Models of electrical conduction processes in both crystalline (c) and amorphous (a) In_2Se_3 are proposed on the basis of theoretical calculations of electronic structures and experimental estimations of valence-band and core-level structures by photoelectron spectroscopy. In a-In_2Se_3 the electrical conduction is found to take place by the thermally activated processes in which the activation energy is evaluated to be ~ 0.4 eV. The observation of an optical gap of 1.6 eV suggests that a-In_2Se_3 can be regarded as an extrinsic semiconductor. The energy-band structures of c-In_2Se_3 are calculated by using the tight-binding method on the two polymorphs; in the β phase all In atoms occupy tetrahedral sites and in the α phase about 6% of In atoms occupy octahedral sites. The semiconductive behavior of the α phase is explained from the calculated band gap of 1.3 eV. Metallic behavior in electrical conduction of the α phase can be explained as originating from an overlap between the valence band and the extended and pseudoconduction band appearing at the midgap of the α phase. The extended states are found to originate from the minor structural components of octahedrally coordinated In atoms. The electronic structure of amorphous states is assumed to be almost the same as that of the α phase based on the results of photoelectron emission measurements. The semiconductive behavior in amorphous states is interpreted by considering the localized nature of band tails. Conduction takes place by thermal activation from the valence and extended states; this model confirms the anomaly in activation energy for conduction in a-In_2Se_3.

I. INTRODUCTION

Since the 1960s amorphous semiconductors have been widely investigated because of potential applications for electronic and optical devices. Amorphous semiconductors can be classified into two groups: amorphous tetrahedral materials such as amorphous silicon and amorphous germanium belong to the first category and chalcogenide glasses such as amorphous selenium and amorphous As_2Se_3 are in the second group. Much progress has been made in the science and technology of the tetrahedral systems after the pioneering work of LeComber and his co-workers.[1,2] They showed that the electrical conductivity and conduction type (p or n) of hydrogenated amorphous silicon can be arbitrarily controlled by the substitutional doping technique. On the other hand no remarkable change in electrical properties has been observed for the chalcogenide glasses doped with a variety of impurities, despite the fact that the effect of doping on electrical conduction was examined on a wide composition region and/or glass-forming systems.[3–6] The experimentally evidenced disadvantage of chalcogenide glasses, failure of the doping, can be explained by the following two reasons. The first is that the requirement of local structure around a dopant to accommodate its normal valency is satisfied.[7] Therefore, the impurities do not form any active level as a donor or an acceptor in an energy gap. The second explanation is related to the existence of specific structural defects in host glasses.[8–10] The defects form discrete levels near the midgap and hence the Fermi level is pinned near the gap center. As a consequence, electrical conduction in most chalcogenide glasses follows that of an intrinsic semiconductor, where the thermal activation energy for conduction (E_σ) is nearly equal to one-half of the energy gap (E_g), i.e., $E_\sigma \cong E_g/2$.[11]

In preceding papers of this series,[12–14] we focused our interest on the second reason and reported the characteristics, geometrical structures, and formation process of the defects in chalcogenide glasses. It was clarified that the existence of electrically neutral defects should be noted as well as charged defects, i.e., valence alternation pairs (VAP).[10] While the existence of VAP has not been experimentally evidenced, several kinds of neutral defects have been observed. For example, paramagnetic defects associated with sulfur, —S·, germanium, ≡Ge·, and arsenic, =As·: have been observed by ESR spectroscopy in the glasses of Ge—S and Ge—As—S systems.[13] Homopolar bonds, —S—S—, ≡Ge—Ge≡, and =As—As= have also been detected by Raman spectroscopy.[12] In addition, "lone-pair electrons on chalcogen atoms with repulsive interactions" have been proposed as a new kind of defect species which give rise to the discrete levels in band gaps.[14] It was stressed that one of the principal factors which affect formation of the defects in chalcogenide glasses is the molecular character of chemical bonds in the system. The molecular character determines the recombination rate between radical species under cooling processes from a melt to a glass; it is an essential condition to determine whether the radicals existing in melts survive in glassy solids through cooling processes.

On the basis of the above-mentioned viewpoint, the failure to control the conductivity and conduction type in chalcogenide glasses by the substitutional doping can also be explained in terms of the molecular character. Principles of the substitutional doping in crystalline silicon is considered to be the requirement of the total free energy to be at a minimum. Thus the crystalline lattice forces the dopant, which substitutes a host atom, to form an unstable valence state forming donor or acceptor levels. On the other hand, the molecular character of chalcogenide glasses allows incorporated impurities to take the most stable valence state, since the molecular character or weak intermolecular bond lowers the barrier of atomic rearrangements. Most of the previous works which aimed to control electrical conduction by the doping technique dealt with glasses with more or less molecular character in which the main constituent elements are group-IV, -V, and -VI atoms of the Periodic Table. It, therefore, seems necessary to choose a system from the viewpoint of the characteristics of chemical bonds in order to have control over the electrical properties of chalcogenide glasses.

Recently, anomalous behavior in electrical properties has been found in the amorphous indium-selenium system.[15–20] Especially for amorphous indium triselenide, In_2Se_3 (hereafter referred to as a-In_2Se_3), variable-range hopping conduction has been observed at low temperature[19,20] and the thermally activated conduction process becomes dominant above room temperature.[18] In both cases, a sign of the Seebeck coefficient is negative, suggesting that a-In_2Se_3 is an n-type semiconductor. Furthermore, the experimentally estimated activation energy for the thermally activated conduction process ($E_\sigma = 0.4$ eV) was found to be far less than one-half of the optically estimated energy gap ($E_g^{\rm opt} = 1.6$ eV). Watanabe *et al.*[18] proposed a conduction mechanism in which the conduction electrons are supplied from donorlike localized states located at about 0.4 eV below the conduction band, structural models of the donor being unspecified. The conduction behavior of a-In_2Se_3 is not observed for other chalcogenide glasses, but often noted in tetrahedral materials such as a-Si:H, which has less molecular character than the chalcogenide glasses. Thus a-In_2Se_3 is an attractive material from a viewpoint to control conduction behavior of amorphous chalcogenides. However, because of the lack of information on the geometrical and electronic structure of a-In_2Se_3, a detailed explanation of the conduction mechanism has not yet been proposed.

In this paper, we report results of investigations on the conduction mechanism of a-In_2Se_3 which are based on an analysis of the electronic structure of crystalline In_2Se_3 (c-In_2Se_3). First, the anomalous behavior in the electronic conduction of a-In_2Se_3 is reconfirmed experimentally. Second, electronic energy-band calculations are carried out for several kinds of crystalline phases of In_2Se_3. Much attention is especially focused on the low-temperature form of c-In_2Se_3 (the α phase) in which metallic conduction had been observed.[21] Then, by assuming that the geometrical structure for a-In_2Se_3 resembles its corresponding crystalline phases, an interpretation about the characteristic conduction behavior is given within the discussions on the electronic structure of this system. It will be elucidated that in a-In_2Se_3 slight deviations from the most stable configuration for indium atoms cause the appearance of extended states in the midgap region where electronic conduction can take place by thermal activation of conduction electrons from the valence band.

II. EXPERIMENTAL PROCEDURES

A. Preparation of amorphous In_2Se_3 thin films

Thin films of amorphous In_2Se_3 were prepared by vacuum evaporation. As done by previous workers, we utilized the flash evaporation technique, since the deviation from the nominal composition of raw materials during evaporation was suppressed to some extent by this method. The raw materials for evaporation were prepared as follows. Elemental indium of 99.99% purity and selenium of 99.9999% purity were carefully weighted for desired composition and the mixture was placed in a silica glass ampoule. The ampoule was evacuated up to 10^{-4} mm Hg, sealed, and heated in an electric furnace equal to 900–1000 °C for more than 24 h. After heating, the ampoule was quenched in an ice-water bath. Then the raw materials were powdered by grinding and sieved to have a mean diameter of 0.5 mm. The powdered raw material in limited amounts was supplied into an alumina-coated tungsten basket heated up to 1200 °C in a vacuum chamber. Films of a-In_2Se_3 were deposited on an optical grade glass substrate under vacuum of less than 10^{-5} mm Hg. The glass substrate was placed about 150 mm distant from the heated basket and was kept at room temperature during deposition.

The film thickness was measured with a multiple-beam interferometer and was about 1.5 μm for most of the films. From the results of the thickness measurement, the deposition rate was calculated to be about 0.05 μm/min X-ray diffraction spectra for the films showed characteristic halo patterns so that the films were recognized as amorphous. The compositions of films were determined by using energy-dispersive analysis of x rays. Though there is an advantage in the flash evaporation technique, slight deviation of composition during evaporation could not be avoided. A series of raw materials, therefore, having different composition was used for evaporation to find out the stoichiometric composition. Thus the films of composition of In_xSe_{100-x}, where x ranged from 35 to 44, were obtained. In each film, the Se content was found to decrease after the flash evaporation and the optimum composition of raw materials to obtain the films of $x = 40$ was found to be $x = 32$.

B. Optical, electrical, and photoemission measurements

Optical-absorption spectra for a-In_xSe_{100-x} films were measured with a Jasco UVIDEC-610C double-beam spectrophotometer in order to evaluate the optical gaps of the samples. The values of $(\alpha h\nu)^{1/2}$ calculated from the obtained spectra were plotted against $h\nu$, where α and $h\nu$ represent the absorption coefficient and photon energy, respectively. The optical gap $E_g^{\rm opt}$ was then determined as the intercept with $(\alpha h\nu)^{1/2} = 0$ in the above plot.

For electrical measurements, a pair of gold electrodes

was attached on samples in coplanar geometry by vacuum evaporation. Direct current conductivity measurements were carried out in an evacuated, light-shaded chamber to eliminate the effects of moisture and photoconduction.

Valence-band and core-level x-ray photoemission spectra (XPS) for crystalline and amorphous In_2Se_3 were recorded on a Shimazu ESCA 750 photoelectron spectrometer utilizing Mg $K\alpha$ radiation ($h\nu=1253.7$ eV). Because of the relatively low-emission efficiency of the valence electron, multiple scanning and signal-averaging treatments were carried out with a microcomputer system attached to the spectrometer.

C. Calculation of energy bands for crystalline indium selenide

Electronic energy bands for c-In_2Se_3 were calculated using a tight-binding method which enables one to analyze the results in terms of constituent atoms. As was stated in the last paragraph of the Introduction, the low-temperature form of c-In_2Se_3 (the α phase) was taken into account [hereafter we refer to it as c-$In_2Se_3(\alpha)$]. It has been found by Semiletov[22] that the structure of c-$In_2Se_3(\alpha)$ is based on two-layer hexagonally packed arrays of selenium atoms. Indium atoms occupy holes in the arrays ($a=16.00$, $c=19.24$ Å; space group $C6$-$C3$; $z=32$). Figure 1 shows $\frac{1}{16}$ part of a unit structure of c-$In_2Se_3(\alpha)$ and hexagonal CdSe, projected on an a-c plane. As seen in the figure, the structure of c-$In_2Se_3(\alpha)$ resembles wurtzite except that the $\frac{1}{3}$ of the sites of indium atoms is empty in order to preserve charge neutrality. Though all indium atoms are tetrahedrally coordinated by four selenium atoms in Fig. 1, 6.25% of indium atoms in the crystal actually occupy octahedral holes so that the structure shown in Fig. 1 is an approximate description of the structure of c-$In_2Se_3(\alpha)$. Then, the approximate structure shown in Fig. 1 is first used in the energy-band calculation in order to clarify the major features of the electronic structure and then, the effects of minor-component, octahedrally coordinated indium atoms are examined.

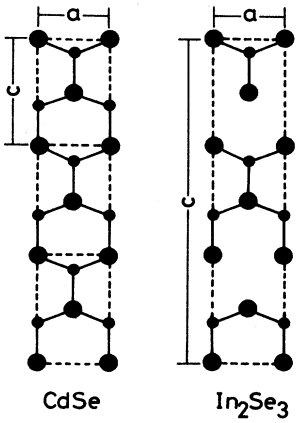

FIG. 1. Crystal structure of CdSe (wurtzite) and In_2Se_3 projected on the a-c plane. Small circles and large circles represent metal and selenium atoms, respectively. The lengths of a and c are 4.3 and 7.02 Å for CdSe, and 4.0 and 19.24 Å for In_2Se_3.

For energy-band calculations with the tight-binding method, atomic orbitals of In 5s, In 5p, Se 4s, and Se 4p were taken as a basis set, χ, to build the one-electron Bloch orbital Φ of the form

$$\Phi(r)=N^{-1/2}\sum_{l,m}\exp[ik(R_l+r_m)]\sum_n c_n\chi_n(r+R_l+r_m)\ , \tag{1}$$

where N, R_l, r_m, and c_n represent the total number of atoms, all of the lattice vectors, vectors of atoms in one unit cell, and linear combination of atomic orbitals (LCAO) coefficients for basis functions. One-electron energies E and the LCAO coefficient c_n at a specific wave vector k were determined by solving the secular equation of the form

$$|H_{ij}-E\delta_{ij}|=0\ , \tag{2}$$

where the matrix elements H_{ij} represent the expectation values for the one-electron Hamiltonian, $\langle\chi_i|\mathcal{H}|\chi_j\rangle$. The H_{ij} were evaluated after dividing the one-electron Hamiltonian into two parts: phase factor P_{ij} and interaction integrals V_{ij}. The interaction integrals V_{ij} were basically evaluated by a method proposed by Harrison *et al.*[23,24] in which the two-center interacting terms ($r_i\neq r_j$) were assumed to be inversely proportional to the square of bond length. In practice, we used the parameters tabulated by Robertson who calculated the electronic structure for indium (II) selenide, InSe, by the same method.[25] In that calculation the one-center parts, H_{ii} were taken to have empirical values comparable to Hartree-Fock atomic energies. The two-center parts V_{ij} were evaluated from two formulas which were used properly with respect to the distance d between two atoms. For distance d smaller than some critical value, d_c, defined for some pairs of atoms, V_{ij} were calculated by the following formula:

$$V_{ij}=U_{ij}/d^2\ . \tag{3}$$

When d became larger than d_c, V_{ij} were evaluated by another formula:

$$V_{ij}=U_{ij}/d^2\exp[\alpha_{ij}(d_c-d)/d_c]\ . \tag{4}$$

Here, U_{ij} and α_{ij} are parameters depending upon the symmetries for the pairs of atoms. In Table I, values for H_{ii} and parameters for V_{ij} were summarized. The critical values d_c were taken to be 2.34 Å for Se-Se, 2.6 Å for

TABLE I. Parameters used in present calculations.

One-center part
$H_{ii}=\langle x_i|\mathcal{H}|x_i\rangle$

x_i	In 5s	In 5$p_{x,y}$	In 5p_z	Se 4s	Se 4$p_{x,y}$	Se 4p_z
H_{ii} (eV)	−10.6	−4.1	−3.4	−20.3	−10.5	−10.2

Two-center part
$H_{ij}=\langle x_i|\mathcal{H}|x_j\rangle$

ij	ss	sp	pp	pp
U_{ij}	−6.7	10.1	12.7	−4.2
α_{ij}	4.4	3.4	2.4	4.0

In-Se, and 2.8 Å for In-In paris, respectively. By considering the effective convergence of calculations, interactions between the atoms separated by more than 4.0 Å were ignored.

The density of states $N(E)$ was also calculated as an ensemble of electronic energy states in the first Brillouin zone, by the following formula:

$$N(E)=1/N\sum_{n}\sum_{k}\delta(E-E_n(k)) , \quad (5)$$

where n and k represent band indices and wave vectors in the first Brillouin zone. DOS for the Γ point were analyzed in terms of contributions of atomic basis orbitals.

III. RESULTS AND DISCUSSION

A. Electrical conduction in a-In_2Se_3

Figure 2 shows the temperature dependence of electrical conductivity for amorphous In_xSe_{100-x} films, where x varies from 35 to 44. As seen in the figure, the conduction in a-In_xSe_{100-x} is a thermal-activation type. The activation energy is evaluated to be about 0.4 eV for the films after fitting each data into the Arrhenius formula by the least-squares method. Composition dependence of the conductivity is slight within the composition range studied in the present report. The results almost agree with the previous works except for the composition dependence of both conductivity and activation energy. Watanabe *et al.* reported that the highest conductivity and the lowest activation energy were observed for a-$In_{40}Se_{60}$ and the changes in the composition from $x=40$ caused a decrease in conductivity and an increase in activation energy simultaneously. However, the above composition dependence is not observed clearly in the present study, partly due to the relatively narrow range of sample composition. Watanabe *et al.* observed also the variable-range hopping conduction in a-In_2Se_3 at temperatures lower than about 200 K. Although we can not confirm the hopping conduction, the process of thermally activated conduction is considered to be the same as previous works.

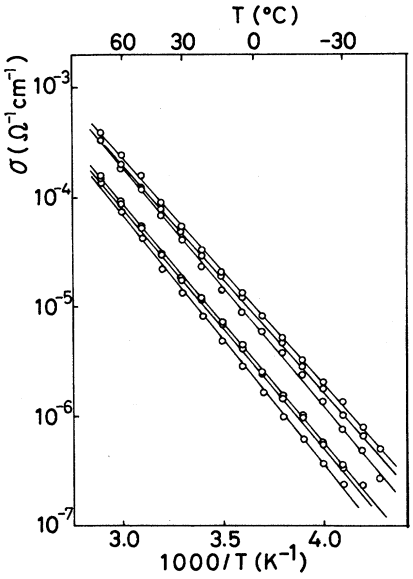

FIG. 2. Changes in conductivity of a-In_xSe_{100-x} thin films with respect to temperature. Here x ranges from 35 to 44.

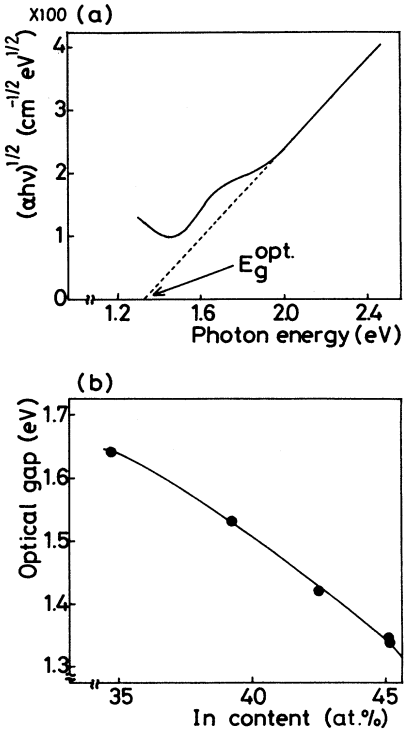

FIG. 3. (a) Optical-absorption spectrum for a-$In_{45}Se_{55}$ thin films plotted on $h\nu$ vs $(\alpha h\nu)^{1/2}$. (b) Composition dependence of an optically estimated energy gap E_g^{opt} for a-In_xSe_{100-x} thin films.

Figure 3 shows (a) the absorption spectrum for the a-

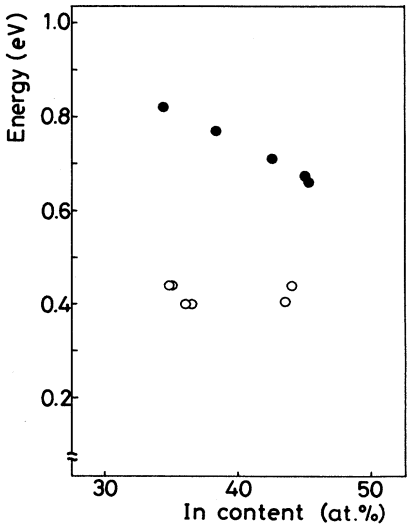

FIG. 4. Composition dependence of activation energy for electrical conduction (○) and for half of an optical gap (●); $\frac{1}{2}E_g^{opt}$ for a-In_xSe_{100-x} thin films.

$In_{45}Se_{55}$ film. $(\alpha h\nu)^{1/2}$ is plotted as a function of $h\nu$. The optical energy gap, E_g^{opt}, is evaluated from the intercept at $(\alpha h\nu)^{1/2}=0$, and its composition dependence is also given in (b). As seen in (a), most of spectra show the dispersive oscillation behavior in the low-energy region, due to the interference of multiple reflected lights caused by a difference in refractive indices between a thin-film sample and a glass substrate. Thus the least-squares method is applied to evaluate E_g^{opt} only in the higher-energy region where the effects of interference are negligible, as shown in (a) by the dashed line. As seen in (b), the values of E_g^{opt} decrease continuously with increasing indium content. The values of E_g^{opt} for crystalline In_2Se_3 and InSe were reported to be 1.42 and 1.29 eV, respectively.[26] It is found that the E_g^{opt} for a-In_xSe_{100-x} films is comparable or slightly larger than those of corresponding crystalline indium selenides.

Figure 4 shows the relationship between the activation energy for electrical conduction E_σ (open circles), and one-half of the optical gap $\frac{1}{2}E_g^{opt}$ (solid circles) for a-In_xSe_{100-x} films plotted against indium content. E_g^{opt} shows a distinct composition dependence, while there is only slight change in E_σ. As was mentioned in the Introduction, an empirical relation, $E_\sigma=\frac{1}{2}E_g^{opt}$, holds for most chalcogenide glasses. Then, the difference between $\frac{1}{2}E_g^{opt}$ and E_σ in a-In_xSe_{100-x} implies that the conduction mechanism in a-In_xSe_{100-x} differs from that in most of chalcogenide glasses. In the following subsections, we will discuss the electronic structure and conduction processes in both crystalline and the amorphous In_2Se_3.

B. Major features of electronic structure for crystalline In_2Se_3

In this subsection, results of the energy-band calculation for crystalline In_2Se_3 are given and analyses of electronic structure are carried out on the basis of decomposition of density of states into the basis atomic functions. It will be clarified that the electronic structure of c-In_2Se_3 differs from the structures of typical chalcogenides such as a-Se and a-As_2Se_3, especially at the near-gap region.

First we calculated the energy band of crystalline In_2Se_3 having the approximate structure shown in Fig. 1, in which all indium atoms are tetrahedrally coordinated. The structural difference between the model structure and actual structure of c-$In_2Se_3(\alpha)$ is the existence of octahedrally coordinated indium atoms with the concentration of 6.25% in the latter. The minor difference seems to be negligible for an analysis on major features in the electronic structure. Figure 5 shows a calculated energy-band structure for the model structure of c-In_2Se_3 drawn in the selected symmetrical directions of wave vector k in the first Brillouin zone, which is also shown in the figure. The band consists of four subbands and the energy gap appears at the shaded region. Both the highest occupied level and the lowest unoccupied level are found at the center of the first Brillouin zone (Γ) with the energy separation of 1.3 eV. Though the calculated energy gap (1.3 eV) is smaller than that of the experimentally determined energy gap, 1.42 eV, of c-$In_2Se_3(\alpha)$, the

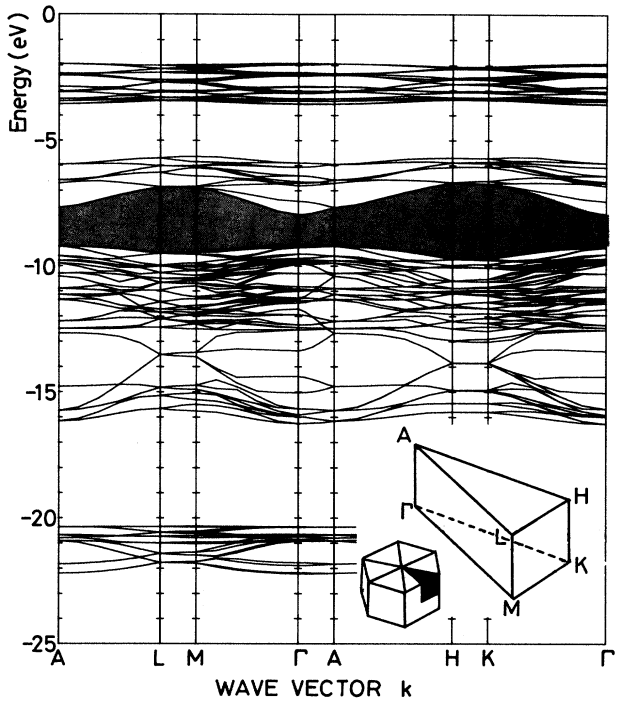

FIG. 5. Energy-band structure of c-In_2Se_3 in which all indium atoms are assumed to be tetrahedrally coordinated as in Fig. 1. Shaded area represents an energy-gap region. The first Brillouin zone is illustrated in the lower right portion. Energy scale on the vertical axis is taken to be normalized to Hartree-Fock atomic energies assumed in the calculation.

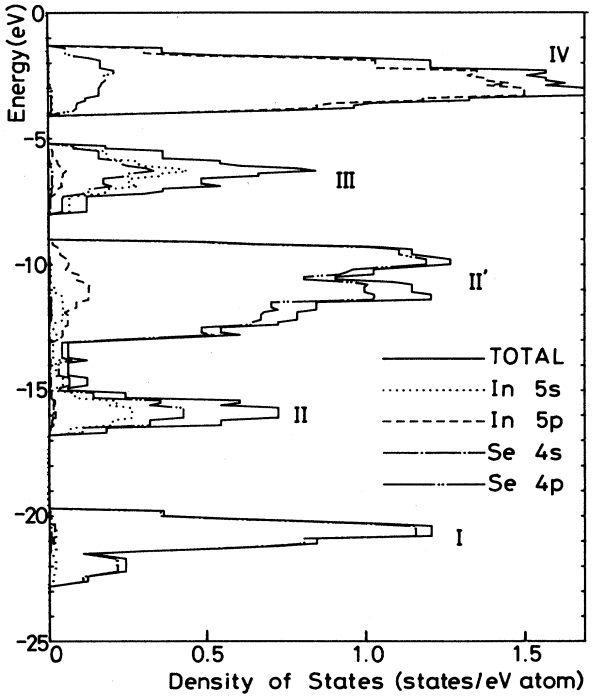

FIG. 6. Calculated density of states (DOS) at the center of the first Brillouin zone (Γ) for c-In_2Se_3, including only tetrahedrally coordinated In atoms. The DOS curve (solid line) is decomposed into contributions of atomic basis functions assumed in the calculation.

calculated electronic structure seems to be a reasonable expression, when considering the validity of the tight-binding approximation.

The above-described energy band for the model c-$In_2Se_3(\alpha)$ was analyzed to assign the origin of each subband to chemical bonds in the system. Figure 6 shows the calculated density of states at the Γ point. In this figure, the solid line represents the total DOS, while the dotted, dashed, dot-dashed, and double-dot–dashed lines represent the contributions of atomic orbital components of In 5s, In 5p, Se 4s, and Se 4p levels, respectively, to the total DOS. For a clear description of bond characteristics, a smoothing treatment was carried out by assuming that each discrete level at Γ had an energy width of 1 eV. As seen in the figure, the origins of four bands are interpreted as follows. (i) The lowest band labeled I is assigned to isolated levels of Se 4s orbitals which hardly takes part in bonding with neighboring indium atoms. (ii) Both the bands labeled II and II′ are assigned to bonding levels between indium and selenium. Band II consists of superposition of In 5s and Se 4p orbitals, while band II′ consists of Se 4p and In 5p orbitals. The degree of the overlapping is higher in band II than band II′ so that the bonding in band II has more covalent nature than bonding in band II′. (iii) Bands III and IV are assigned to antibonding levels corresponding to bands II and II′, respectively. Hereafter, we use a notation for designation of electronic states as follows: nonbonding, bonding, and antibonding states are represented by n, σ, and σ^*, respectively. For each of the states, atomic orbitals forming the state are specified by the subscript. Therefore, bands I, II, and III are represented by n_p, σ_{sp}, and σ^*_{sp}, respectively. Here, the first letter in the subscript is the atomic orbital of metal atom and the second is that of nonmetal atom. It is noted that for nonbonding states, the subscript represents the atomic orbitals of nonmetal.

From the above-discussed assignment, it is found that the electronic structure of c-$In_2Se_3(\alpha)$ is essentially different from that of other chalcogenides of group-IV and -V elements. For example, the electronic structures of c-Se and c-As_2Se_3 have common features;[27] the highest occupied bands arise from lone-pair electrons on chalcogen atoms (n_p). These lone-pair electrons are occupying nonbonding states localized on chalcogen atoms. On the other hand, the highest occupied band in c-$In_2Se_3(\alpha)$ is bonding states (σ_{pp}). This fact suggests that a delocalization of valence electrons is not negligible. Furthermore, another difference in the electronic structure can be found in the origin of the lowest unoccupied band. The lowest unoccupied bands in c-Se or c-As_2Se_3 and c-In_2Se_3 are antibonding states. However, the bands are compared of only p orbitals (σ^*_{pp}) in the former systems, while in c-In_2Se_3 s orbitals of metal and p orbitals of chalcogen form the band (σ^*_{sp}). The incorporation of s orbital contributes to a relatively large dispersion of energy with respect to wave vector k, i.e., dE/dk, since the width of specific bands are basically determined by the number and the magnitude of interaction term $\langle \chi_i | \mathcal{H} | \chi_j \rangle$. The distribution of electrons in the s orbital is spherically symmetric and that in the p orbital is axially symmetric. Though the degree of an interacting term between p orbitals $\langle \chi_{pi} | \mathcal{H} | \chi_{pj} \rangle$ is generally larger than that of s orbitals, higher symmetry of the s orbital results in a larger number of interaction terms which contribute to width of the band. Thus, a large energy dispersion due to the incorporation of In 5s orbitals in c-$In_2Se_3(\alpha)$ is notable. It is needless to say that mobility of a conduction electron is closely related to dE/dk.

C. Refinement of electronic structure for c-$In_2Se_3(\alpha)$ with inclusion of six-coordinated In atoms

In Sec. III B, we dealt with the electronic structure of the model structure of c-$In_2Se_3(\alpha)$. From the above discussions, one can expect an intrinsic semiconductive behavior of c-$In_2Se_3(\alpha)$, where the thermal-activation energy for electrical conduction is one-half the optical gap. However, as was mentioned in the last paragraph of the Introduction, c-In_2Se_3 of the α phase shows metallic features in electrical conduction. In this section, the electronic structure for real crystalline In_2Se_3 of the α phase is discussed and conduction processes for both crystalline and amorphous In_2Se_3 are proposed after the discussion on nature of gap states.

In real structure of c-$In_2Se_3(\alpha)$, there exist octahedrally coordinated indium atoms with the concentration of 6.25 at.%, besides the tetrahedrally coordinated atoms. Then, metallic behavior in the electrical conduction of c-$In_2Se_3(\alpha)$ must be attributed to the existence of octahedrally coordinated indium atoms, since the model structure of c-$In_2Se_3(\alpha)$ should be a semiconductor in the absence of the six-coordinated In atoms. Actually, semiconductive behavior was observed at above 200 °C, where a phase transition takes place from the α phase to the β phase. In the β phase of c-In_2Se_3, there are no six-coordinated In atoms[28] so that the resulted electronic structure obtained in Sec. III B seems to agree with that of c-$In_2Se_3(\beta)$.

Figure 7 shows the structural relation between six-coordinated indium atoms and four-coordinated indium atoms. As seen in (a), a hexagonally close-packed structure of selenium atoms has both tetrahedral and octahedral holes in between the two adjacent layers with the ratio of 2:1. It is suggested that indium atoms can be converted to the six-coordinated sites from the four-coordinated sites only with slight deviation, as shown in (b). One significant difference after the structural conversion appears in bond length between the indium atoms and selenium atoms; the bond length for six-coordinated In becomes about 1.2 times larger than that of four-coordinated In.

Energy-band calculations were then carried out in order to examine how the six-coordinated indium atoms modify the electronic structure of c-In_2Se_3. Results are presented in Fig. 8 where the concentration of six-coordinated indium atoms is chosen to be 6.25% in (a) as well as that in the real crystal. For comparison, Fig. 8(b) shows the result of similar calculations on the model in which the concentration of six-coordinated In is increased artificially to 25%. As noted in Fig. 8(a), major features in the E-k diagram are almost similar with those of Fig. 5 even after the inclusion of six-coordinated indium atoms. The E-k dispersion of the shaded area in Fig.

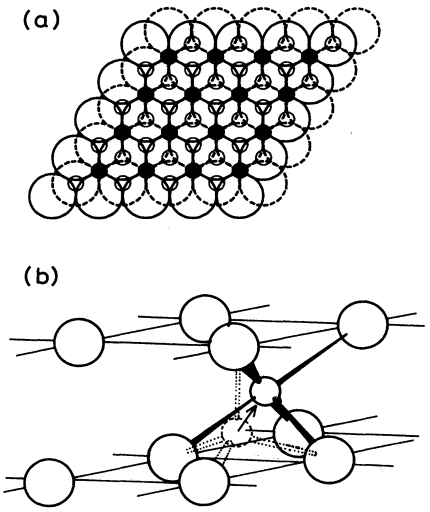

FIG. 7. (a) Hexagonally packed arrays of selenium atoms (large circles) and the holes occupied by In atoms with tetrahedral (small open circles) and octahedral (small closed circles) coordination. (b) Schematic illustration of conversion from tetrahedrally coordinated to octahedrally coordinated In atoms.

7 is similar, especially to the energy-gap region in Fig. 5. However, a new band labeled V appears in the shaded region as indicated by an arrow. Band V is also found in (b), where the band shows complicated structure. The band V is found to be in unoccupied states. Therefore, the shaded regions in Fig. 8 are not energy gaps and the true energy gaps are the shaded regions below band V. The smallest gap energies are found at Γ and were 0.4 eV in (a) and 0.2 eV in (b), respectively. The changes in the shape and the increase in width of the Vth band with increasing six-coordinated indium atoms strongly suggest that the band V originates from six-coordinated indium atoms.

In order to assign the origin of band V, E-k diagrams of Fig. 8 were converted to DOS's and the DOS's were further decomposed into contributions of the basis atomic orbitals. Figure 9 shows the DOS at Γ for c-$In_2Se_3(\alpha)$ in which the six-coordinated In atoms are assumed to be present by 25% [corresponding to Fig. 8(b)]. Main features labeled I, II, II′, III, and IV survive even after the inclusion of six-coordinated In atoms. As was noted in the last paragraph, the most striking change in the electronic structures is the appearance of band V and this is again confirmed in the DOS diagrams in which one can see the relatively high density of states for the Vth band. Moreover, some changes caused by inclusion of six-coordinated In atoms can be observed by comparing the shaded regions labeled V′ and IV′ in Fig. 9 with Fig. 6. The new features in DOS are observed in the case in which the concentration of six-coordinated In atoms is assumed to be 6.25% as well as in real crystal. However, reduction in the DOS of the newly appearing bands, V, V′, and IV′, is observed.

From the results shown in Fig. 9, the origin of band V can be interpreted as follows. First, band V consists of In 5s and Se 4p orbitals, the former being dominant. This is similar to band III which has already assigned to antibonding states of the In—Se bond (σ^*_{sp}). Therefore, the Vth band is also assigned to the antibonding states $\sigma^{*'}_{sp}$ (here, the superscript prime is used for distinction between four-coordinated and six-coordinated In atom). The lower energy for band V rather than band III indicates that energy of the conjugate bonding bands is smaller than that for band III, since stabilization of antibonding states immediately reflects instabilization of bonding states. This insight is supported by the appearance of band V′ above band II, which are the conjugate σ_{sp}

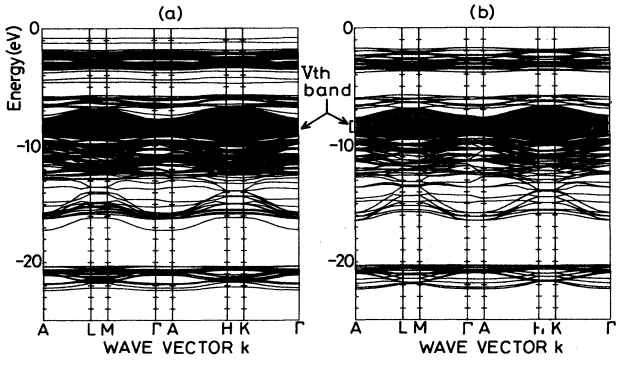

FIG. 8. Calculated energy-band structures of c-In_2Se_3 in which (a) 6.25% and (b) 25% of In atoms are assumed to be octahedrally coordinated. Appearance of the Vth band in an energy-gap region (shaded area) is noted.

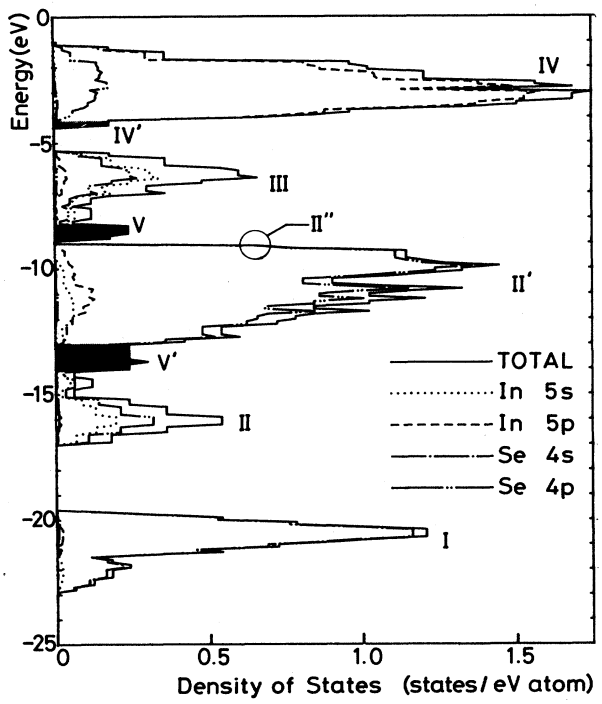

FIG. 9. Calculated DOS at Γ for c-In_2Se_3 including octahedrally coordinated In atoms. Note that shaded parts newly appear after the inclusion of octahedrally coordinated In atoms.

bonds of the band III. Band V′ also consists of In 5*s* and Se 4*p* orbitals as well as band V, while the contribution of these two orbitals is inverted in comparison with that in band V. Thus the band V′ is assigned to the bonding states, σ'_{sp}, corresponding to the antibonding states $\sigma^{*'}_{sp}$, band V. Furthermore, considering the resemblance of construction of bands between V′ and II, it can be considered that In-Se pairs forming band V′ has less binding energy than that of band II. The lowering of binding energy can be interpreted reasonably in connection with the formation of six-coordinated In atoms. Six-coordinated In atoms are formed by small displacement of In atoms from four-coordinated In sites. This formation process is always accompanied by an elongation of the bonds between In and Se atoms and the elongation of the bonds directly causes the lowering of binding energy of the In-Se pair. The remaining band labeled IV′ can also be assigned in a similar manner. Band IV′ is an antibonding state ($\sigma^{*'}_{pp}$) of the In-Se pair, as well as band IV in which In 5*p* and Se 4*p* orbitals are main components. The conjugate bonding states (σ'_{pp}), band II″ are expected to appear just above band II′, but the large DOS of II′ band might hinder the clear distinction of bonding states II″.

Thus, the electronic structure for c-$In_2Se_3(\alpha)$ was fully examined with consideration given to the nature and contribution of the minor structural components, six-coordinated In atoms, to the whole electronic structure. Figure 10 shows a comparison of (a) valence-band XPS spectrum of c-$In_2Se_3(\alpha)$ and (b) the calculated DOS for c-In_2Se_3 in which all indium atoms are in four-coordinated (dashed line) and 25% of indium atoms are in six-coordinated (solid line). In the calculations, the irreducible wedge of the first Brillouin zone shown in Fig. 5 was divided into 64 subzones. As seen in the figure, whole shape and characteristic peaks in the XPS spectrum are well reproduced in the calculated DOS, while the relative intensities of the peaks in the spectrum are in disagreement with the calculated DOS. The disagreements are considered to be related to the low-photoemission efficiency of valence electrons under x irradiation. Furthermore, it should be noted that the peak indicated by an arrow in (a) does not seem to appear clearly in calculated DOS's. However, we assign the peak in Fig. 10(a) to band V′ of Fig. 9 for the following reason. The most striking difference between the two calculated DOS's in Fig. 10(b) appears in the energy region of ≈ -4 to -8 eV where the DOS curves (solid and dashed line) shows the reverse in their intensities. This change can be explained by considering the role of six-coordinated In atoms on the DOS. Because of the long bond length between six-coordinated In atoms and neighboring Se atoms compared with that of four-coordinated In atoms, the electronic energy level due to six-coordinated In atoms is higher than that of four-coordinated In atoms. As discussed before, the peak at -6.5 eV in Fig. 10(b) is assigned to In-Se bonding states in which In atoms are in four-coordinated structure and the peak at -4.5 eV is assigned to that of six-coordinated atoms. Therefore, the reverse in DOS intensity in Fig. 10(b) originates from the existence of six-coordinated In atoms. Thus the peak indicated by an arrow in Fig. 10(a) is assigned to band V′ (six-coordinated In atoms), since the experimental DOS (a) is measured for the α phase and there is no reasonable explanation for the appearance of a peak in the energy region of ≈ -4 to -8 eV in the absence of six-coordinated In atoms.

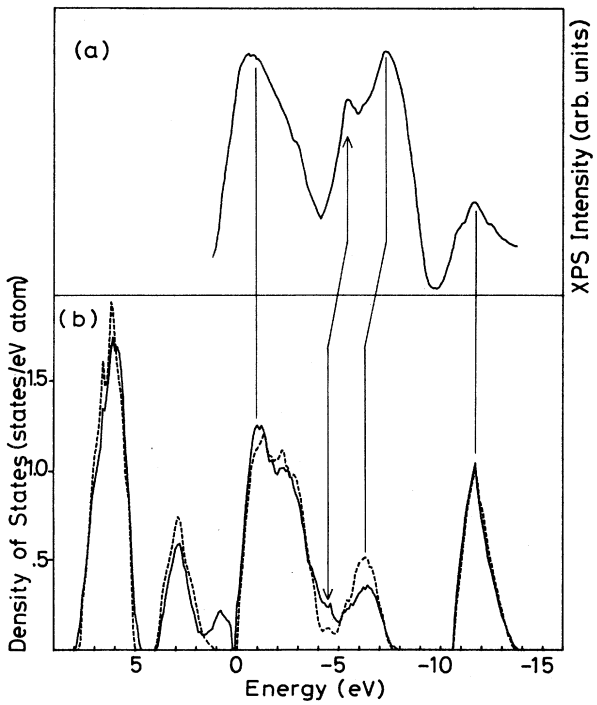

FIG. 10. (a) Valence-band XPS spectrum of c-$In_2Se_3(\alpha)$. (b) Calculated DOS's of c-In_2Se_3 in which the six-coordinated In atoms are assumed to be present by 25% (solid line) and to be absent (dashed line).

Thus the valence-band electronic structure of c-$In_2Se_3(\alpha)$ was examined within the result of photoemission measurements and the calculated DOS's including conduction bands is thought to be supported by the measurements. It should be noted that a principle of valence-band theory supports the existence of band V, since bands V′ and V are always formed in pairs.

D. Conduction process in crystalline and amorphous In_2Se_3

We now discuss the electrical conduction processes in both crystalline and amorphous In_2Se_3 on the basis of knowledges on the electronic structures discussed in Sec. III C.

Only the electronic states near the energy-gap region are important in electrical conduction process. Figure 11 shows a schematic illustration of electronic states for c-In_2Se_3 in the vicinity of the energy gap. In this figure, shaded regions are fully occupied by valence electrons. Both the bands labeled V and II″ originate from six-coordinated In atoms as mentioned in Sec. III C; V and II′ are antibonding states with In 5*s* and Se 4*p*, $\sigma^{*'}_{sp}$ and bonding states with In 5*p* and Se 4*p*, σ'_{pp}, respectively. In the results of the calculations shown in Fig. 8, energy gaps of 0.2–0.4 eV appeared between band V and the

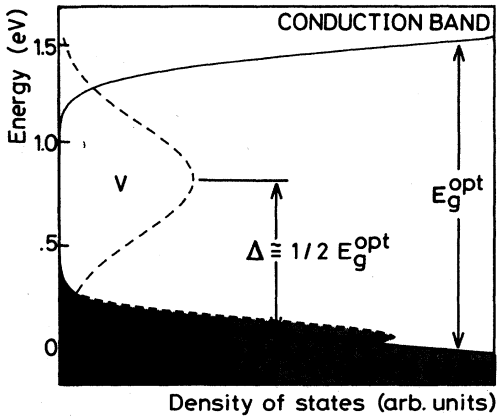

FIG. 11. Schematic illustration of DOS for c- and a-In_2Se_3 at the near-gap region. Shaded area represents occupied states.

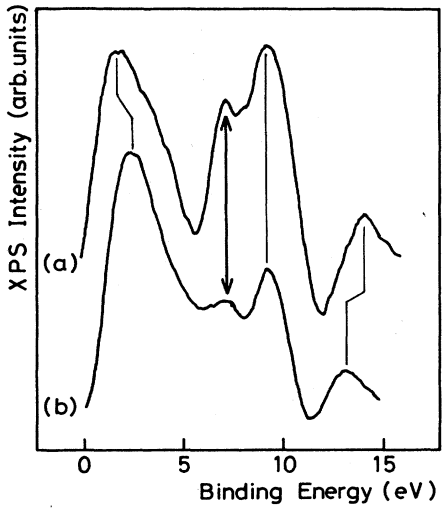

FIG. 12. Comparison of valence-band XPS spectrum between (a) crystalline and (b) amorphous In_2Se_3. Appearance of the peak indicated by arrows in (b) indicates the existence of octahedrally coordinated In atoms even in amorphous states.

valence band. However, we assume in Fig. 11 that band V and the valence band might overlap with each other by some degrees, since such a small gap is very sensitive to a selection of the parameters in tight-binding calculations. Actually, overlap of these two bands could be produced, when the two-center interaction terms $\langle \chi_i | \mathcal{H} | \chi_j \rangle$ were overestimated. Thus, metallic conduction behavior in c-$In_2Se_3(\alpha)$ is interpreted as that the conduction electrons pass through the overlap region as well as typical metals. In this case, the lower density of states at the overlap region than general metals restricts the free motion of conduction electron. This results in the relatively low conductivity in the order of $10^3\ \Omega^{-1}\,m^{-1}$.

Upon discussions on electrical conduction in a-In_2Se_3, we must consider the geometrical structure of a-In_2Se_3. Raman studies on the structure of amorphous In-Se films have revealed that the local structure in amorphous thin films is similar to that in the crystal.[18] On the other hand, it has been reported that the bulk c-In_2Se_3 samples prepared by rapid cooling of the melt contains α and other high-temperature phases.[29] These facts indicate that the short-range order in the geometrical structure is similar between c- and a-In_2Se_3. The similarity of short-range order in both phases suggests the resemblance in main features of electronic structures. Figure 12 shows valence-band XPS spectra for (a) c-$In_2Se_3(\alpha)$ and (b) a-In_2Se_3. As seen in the figure, whole shape and characteristic peaks in c-$In_2Se_3(\alpha)$ are well observed also in a-In_2Se_3. It should be noted that the peak of band V′ in (a) is clearly observed even in the amorphous states (b). Furthermore, the agreement in peak positions of the first two core levels, In 4d and Se 3d, between c- and a-In_2Se_3 was confirmed by XPS measurements. Therefore, we assume that the electronic structure for c-$In_2Se_3(\alpha)$ can essentially be adopted as that for a-In_2Se_3.

As was described in Sec. III A, electrical measurements on a-In_2Se_3 films confirmed semiconductive behavior. This fact seems to be inconsistent with the above assumption which suggests that a-In_2Se_3 should possess metallic conduction behavior as well as c-$In_2Se_3(\alpha)$. Watanabe *et al.* proposed that the conduction electrons under the thermal-activation process in a-In_2Se_3 were supplied from donorlike localized states at about 0.4 eV below the conduction-band edge. However, this model seems to be unacceptable according to the following reasons. First, the structural assignment of the defects (or impurities) forming donor levels was not clear. Secondly, the saturation behavior in a temperature dependence of electrical conduction must be observed in the model. In other words, a number of carriers excited from the donor levels does not change so much with changes in the temperature near room temperature. Thus, according to this process, the apparent activation energy for conduction evaluated from $\log_{10}\sigma - 1/T$ plot must be smaller than the energy difference between the donor level and conduction band.

Here, we propose an alternative model for electrical conduction processes in a-In_2Se_3 by considering how the electronic structure is modified by lack of the structural periodicity. Generally, one of the major characteristics of the band structures of amorphous semiconductors is the existence of localized states in the band tails. Then, turning to DOS diagrams for a-In_2Se_3 in Fig. 11, the edges of conduction and valence band are considered to be localized states. Bands V and II″ are also considered to have localized nature at each band tail. In the localized states, electrons cannot move freely even under application of external electric field so that contributions to conduction are not expected for such localized electrons. Therefore, behavior of metallic conduction in c-In_2Se_3 disappears in the case of a-In_2Se_3, since the overlap regions of band V and the valence band are both localized states. However, the central part of band V has larger density of states than its tail part and seems to have an extended nature to some extent. In this case, thermally activated electrons from the valence band to the center of band V contribute to electrical conduction. As seen in Fig. 11, the difference (Δ) between the edge of the

valence band and the center of band V is nearly equal to $\frac{1}{2}E_g^{\text{opt}}$. Because of the relatively large value of Δ, Fermi levels were pinned near the center of the gap between the peak of band V and the valence band within a large temperature range. This predicts that the activation energy for electrical conduction becomes $\frac{1}{2}\Delta$, or $\frac{1}{4}E_g^{\text{opt}}$. The experimentally observed values for E_σ and E_g^{opt} were 0.4 and 1.7 eV, respectively, and well satisfy the above relationship. Though we state that the DOS of band V is relatively large, capable of modifying electrical conduction, band V gave small modification to the optical-absorption spectrum as for the tailing in the absorption spectrum, since there are far larger differences between DOS's of band V and conduction and/or valence bands. In other words, DOS of band V is effectively large for electrical conduction, but it does not affect so much in optical absorption.

IV. CONCLUDING REMARKS

In the present work, anomalies of electrical properties in a-In_2Se_3 were confirmed and a model of conduction processes in a-In_2Se_3 was proposed. The proposed model for conduction processes seems to resemble that of "impurity conduction" in crystalline silicon in which the heavily doped impurities such as As form the extended "impurity band" at the edge of conduction band. However, in the present model, extended states are not formed by impurities but by a fraction of particular and constituent atoms having different local structures from the major species. Furthermore, in the present model, extended states are empty so that the repulsive interactions between conduction electrons can be less than those in impurity conduction in crystalline silicon, suggesting relatively high mobility for conduction electrons. Further investigation on ultraviolet photoemission spectroscopy measurements is now ongoing to support this model, especially for the elucidation of whether or not the six-coordinated In atoms really exist to some extent in a-In_2Se_3.

As a final remark, it is stated that the extended empty states, band V, might appear incidentally at a center of the band gap for a-In_2Se_3 phases having only tetrahedrally coordinated indium atoms. However, the appearance of such kinds of states can be expected in other amorphous semiconductors, since the structural fluctuations are intrinsic characteristics of amorphous materials. Thus, the present model suggests possibilities for control of electrical properties by positive utilization of these "defect" associated extended states.

[1]P. G. LeComber and W. E. Spear, in *Amorphous Semiconductors,* edited by M. G. Brodsky (Springer-Verlag, New York, 1979).

[2]W. E. Spear and P. G. LeComber, Solid State Commun. **17**, 1193 (1975).

[3]B. T. Kolomiets, Yu. V. Rukhlyadeu, and U. P. Shilo, J. Non-Cryst. Solids **5**, 389 (1971).

[4]B. T. Kolomiets, Yu. V. Rukhlyadeu, and U. P. Shilo, J. Non-Cryst. Solids **5**, 402 (1971).

[5]K. S. Liang, A. Bienenstock, and C. W. Bates, Phys. Rev. B **10**, 1528 (1974).

[6]N. F. Mott, Philos. Mag. **34**, 1101 (1976).

[7]N. F. Mott, Adv. Phys. **16**, 49 (1967).

[8]M. H. Cohen, H. Fritzsche, and S. R. Ovshinsky, Phys. Rev. Lett. **22**, 1065 (1969).

[9]E. A. Davis and N. F. Mott, Philos. Mag. **22**, 903 (1970).

[10]M. Kastner and D. Adler, Phys. Rev. Lett. **37**, 1504 (1976).

[11]N. F. Mott and E. A. Davis, *Electronic Processes in Non-Crystalline Materials* (Clarendon, Oxford, 1979).

[12]H. Kawazoe, H. Yanagita, Y. Watanabe, and M. Yamane, Phys. Rev. B **38**, 5661 (1988).

[13]Y. Watanabe, H. Kawazoe, and M. Yamane, Phys. Rev. B **38**, 5668 (1988).

[14]Y. Watanabe, H. Kawazoe, and M. Yamane, Phys. Rev. B **38**, 5677 (1988).

[15]T. T. Nang, T. Matsushita, M. Okuda, and A. Suzuki, Jpn. J. Appl. Phys. **16**, 253 (1977).

[16]H. Naito, M. Okuda, T. Matsushita, and T. Nakau, Jpn. J. Appl. Phys. **19**, L513 (1980).

[17]M. Okuda, T. Kirimoto, H. Naito, T. Matsushita, and T. Nakau, J. Non-Cryst. Solids **59&60**, 1035 (1983).

[18]I. Watanabe and T. Yamamoto, Jpn. J. Appl. Phys. **24**, 1282 (1985).

[19]I. Watanabe and T. Sekiya, Jpn. J. Appl. Phys. **26**, 633 (1987).

[20]I. Watanabe and T. Sekiya, J. Non-Cryst. Solids **97&98**, 667 (1987).

[21]S. Sugaike, Mineral J. **2**, 63 (1957).

[22]S. A. Semiletov, Kristallografiya **6**, 200 (1961) [Sov. Phys. Crystallogr. **6**, 158 (1961)].

[23]W. A. Harrison, Phys. Rev. B **14**, 702 (1976).

[24]W. A. Harrison and S. Ciraci, Phys. Rev. B **10**, 1516 (1974).

[25]J. Robertson, J. Phys. C **12**, 4777 (1979).

[26]C. Julien, E. Hatzikraniotis, A. Chevy, and K. Kambas, Mater. Res. Bull. **20**, 287 (1985).

[27]M. Kastner, Phys. Rev. Lett. **28**, 355 (1972).

[28]S. A. Semiletov, Kristallografiya **5**, 704 (1960) [Sov. Phys.—Crystallogr. **5**, 673 (1961)].

[29]C. Julien and I. Samaras, Solid State Ionics **27**, 101 (1988).